*Int. J. Electrochem. Sci.*, 7 **(2012)** 437 - 444

International Journal of
ELECTROCHEMICAL
SCIENCE
www.electrochemsci.org

# Novel Spherical $Li_3V_2(PO_4)_3$/C Cathode Material for Application in High–Power Lithium Ion Battery

*Bing Huang*[*], *Xiaodong Zheng, Mi Lu, Su Dong, Yu Qiao*

Clean Energy Research and Development Center, Binzhou University, Binzhou 256603, PR China
[*]E-mail: huangbingbzu@sina.com

*Received:* 4 November 2011 / *Accepted:* 12 December 2011 / *Published:* 1 January 2012

A novel spherical $Li_3V_2(PO_4)_3$/C material is synthesized by modified carbothermal reduction. XRD patterns show that the $Li_3V_2(PO_4)_3$ compound is monoclinic crystal structure. The C 1s XPS core peaks indicate that residual carbon exists in $Li_3V_2(PO_4)_3$. The binding energy values in P 2p and O 1s spectra are attributed to $(PO_4)^{3-}$ phosphate groups and V 2p core peak at 517.2 eV indicate the oxidation state of V is +3. SEM results indicate that the $Li_3V_2(PO_4)_3$/C composite had a spherical morphology with hollow structure and nanosized primary particles. Charge/discharge tests show that as-prepared sample exhibits discharge capacity of 131 mAh $g^{-1}$ at 0.2 C rate in the voltage range of 3.0–4.3 V. The discharge capacities of $Li_3V_2(PO_4)_3$/C are 128, 121, 108, 93, 84 mAh $g^{-1}$ at 1, 8, 15, 25, 35 C rate and high voltage plateaus are achieved. The excellent rate performance of the composite is due to its unique spherical structure, which improves the processability and wetting ability of the $Li_3V_2(PO_4)_3$ electrode, shortens the diffusion length of lithium ions and electrons.

**Keywords:** Lithium-ion batteries; Cathode materials; $Li_3V_2(PO_4)_3$; Rate performance

## 1. INTRODUCTION

Lithium ion batteries (LIBs) have revolutionized the portable electronics market, but in new applications, like hybrid electric vehicles, require a higher charge-discharge rate capability [1,2]. The development of cathode materials with good capacity and capacity retention at high rates is critical in improving the power of a LIB system [3–5].

Monoclinic structure $Li_3V_2(PO_4)_3$ composite has received considerable attention due to its high operate voltage, good ion mobility and high reversible capacity [6–8]. However, as most of polyanion materials, the separated $[VO_6]$ reduces the electronic conductivity of the material, which results in a poor rate capability. Small size particles show enhanced kinetic properties in principle due to short diffusion length for charge carriers and increased reaction area. Benefited from this advantage, high

rate performances have been achieved in the cases of nanosized polyanion phosphate cathode materials [9–13].

However, due to high specific surface, nanosized active material easily aggregate and absorb moisture from the air, and more binder is needed during electrode preparation, all of which are disadvantageous to the electrochemical properties of cathode material.

Here we report on our work to improve the rate performance of $Li_3V_2(PO_4)_3$ materials, by making this material nanostructured, more importantly, the synthesized material with micro-spherical morphology. Through substituting $V_2O_5$ for $NH_4VO_3$ in vanadium source, the spherical morphology is more uniform than in our previous work [14] and the voltage plateau of the micro-spherical $Li_3V_2(PO_4)_3$/C is improved significantly when discharging at high rate.

## 2. EXPERIMENT

### *2.1. Preparation and characterization of $Li_3V_2(PO_4)_3$/C powders*

The stoichiometric amount of $LiH_2PO_4$ (99%) and $V_2O_5$ (99.5%) were dispersed in ethanol and then ball milled for 15 h. The mixtures were dried at 80 ºC, and then transferred into a tube furnace and heated to 350 ºC for 3 h under an argon atmosphere. Then the pre-sintered mixtures and sucrose in the amount of 25 g per mole $LiH_2PO_4$ (about 3 wt.% carbon) were ball milled again in ethanol for 15 h. The ball-milled mixture was dispersed in ethanol to obtain an emulsion, and then spray dried at 120 ºC. The spray dried precursor was then heated to 800 ºC at a heating rate of 5 ºC $min^{-1}$ for 10 h under an argon atmosphere.

The obtained $Li_3V_2(PO_4)_3$/C powder was subjected to X-ray diffraction (XRD, Panalytical X' Pert, Philips) for phase analysis using $CuK_\alpha$ radiation scanned in the range of 10–60º ($2\theta$). X-ray photoelectron spectroscopy (XPS, PHI Quantum2000, Physical Electronics, Inc.) was employed to measure the chemical or electronic state of each element in the surface. Peak fitting was performed using the XPSPEAK software.

The morphology of the $Li_3V_2(PO_4)_3$/C powder was observed by scanning electron microscope (SEM, EM3200, KYKY).

### *2.2. Electrochemistry measurements*

The $Li_3V_2(PO_4)_3$ slurry was prepared via mixing 80 wt.% active material, 10 wt.% carbon black and 10 wt.% polyvinylidene fluoride solution in N-methylpyrrolidone and then was coated onto an aluminum foil over an area of 1 $cm^2$.

The cells (CR2025 coin type) were assembled in an argon-filled glove box (Etelux). The electrolyte was 1 mol $L^{-1}$ $LiPF_6$ in ethylene carbonate/diethylene carbonate/methyl ethyl carbonate (1:1:1, v/v/v). The cells were measured using Neware galvanostatic charge–discharge unit in the voltage range of 3.0–4.3 V.

## 3. RESULTS AND DISCUSSION

### *3.1. Physical characteristics*

The XRD pattern of the $Li_3V_2(PO_4)_3$ powder, shown in figure 1, is similar to the previous reports [6,7]. All the peaks are indexed with monoclinic structure with space group $P2_1/n$ (No. 14). Excess carbon left in $Li_3V_2(PO_4)_3$/C composite was not detected because the residual carbon is amorphous or the thickness of the residual carbon on the $Li_3V_2(PO_4)_3$ powders is too thin [15].

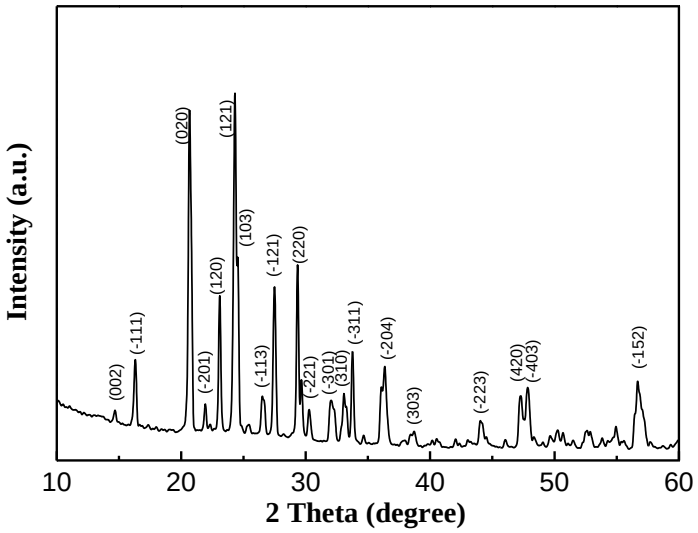


**Figure 1.** XRD pattern of the $Li_3V_2(PO_4)_3$/C composite.

Additionally, XPS is used to testify the compositions and valence of elements in carbon-coated $Li_3V_2(PO_4)_3$ pristine material. Figure 2a shows C 1s core peaks of the $Li_3V_2(PO_4)_3$/C powder. The peak originating from C–C (284.6 eV) bond indicates that sucrose is decomposed into carbon during the calcination, and residual carbon exists in $Li_3V_2(PO_4)_3$ [16].

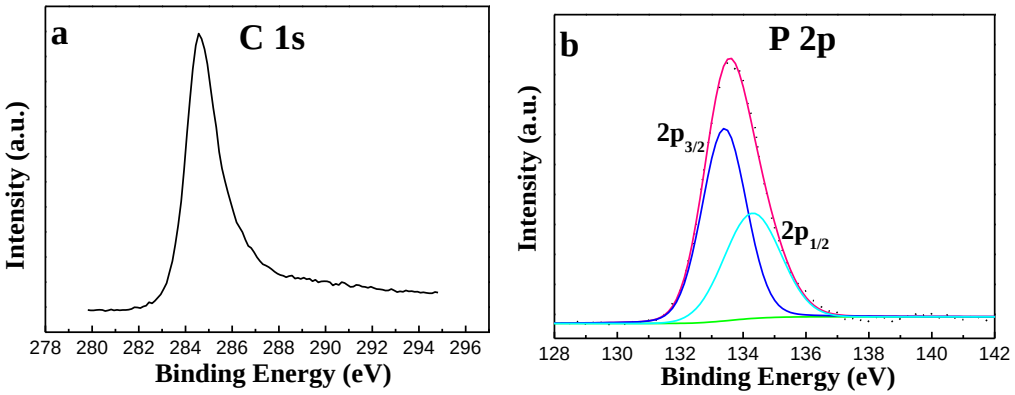

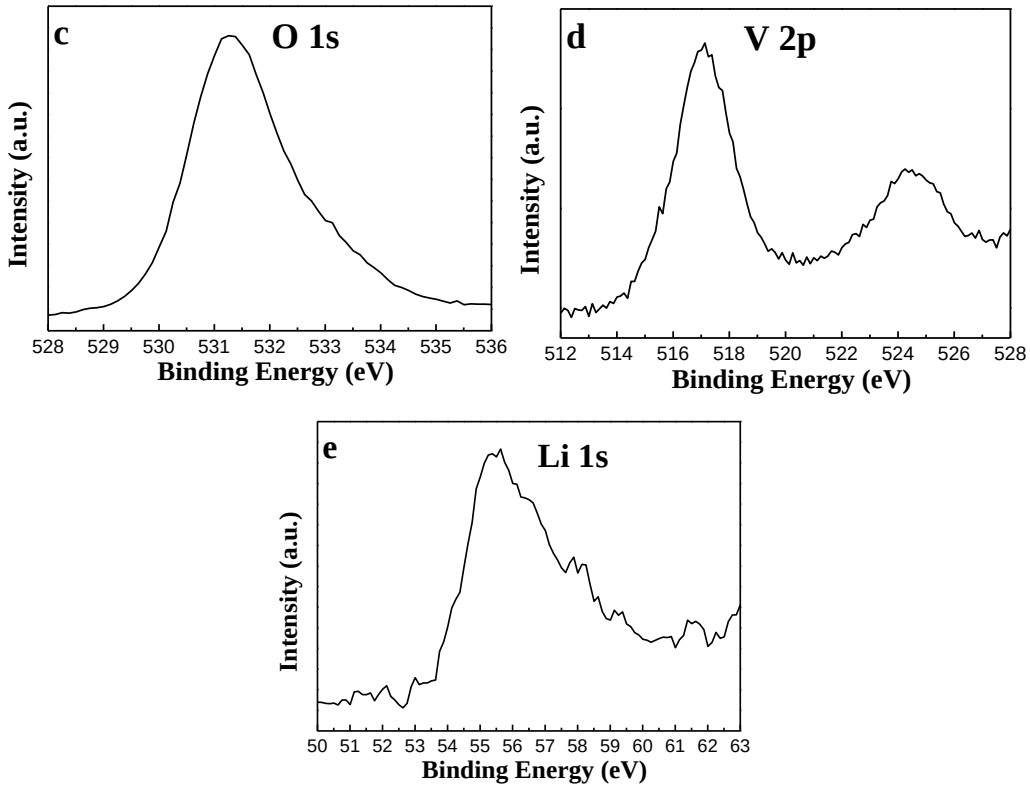


**Figure 2.** XPS spectrum of C, P, O,V, Li of the $Li_3V_2(PO_4)_3$/C composite.

The absence of the characteristic peak at 290 eV confirms the absence of surface $Li_2CO_3$ on our sample [17]. The P 2p spectrum shown in figure 2b is split in two components $2p_{3/2}$ and $2p_{1/2}$ due to spin-orbit coupling (133.4 and 134.3 eV, respectively). Only one P 2p doublet at this binding energy is attributed to $(PO_4)^{3-}$ phosphate group. The O 1s core level shown in figure 2c fits to a single peak with a binding energy of 531.3 eV which is attributed to oxygen atoms of $(PO_4)^{3-}$ phosphate groups. The V 2p core peak shown in figure 2d displays a peak at 517.2 eV, matching well with that observed in $V_2O_3$ (517.2 eV) [18], so the oxidation state of V in $Li_3V_2(PO_4)_3$ was +3. And the Li 1s spectrum shown in figure 2e displays a peak at 55.3 eV can be attributed to $Li_3V_2(PO_4)_3$ [19].

SEM images of precursor powder and $Li_3V_2(PO_4)_3$/C sample are shown in figure 3. Figure 3a shows that the as-prepared precursor powders obtained from spray-drying had a spherical morphology with hollow structure due to instant evaporation of ethanol and a relatively smooth surface. The surface morphology of $Li_3V_2(PO_4)_3$/C, obtained from the precursor, is shown in figure 3b. The as-synthesized $Li_3V_2(PO_4)_3$/C sample remains hollow micro-spherical after heating at 800 °C and is significantly constituted of a large number of nanosized primary particles. The results show that the substitution of $V_2O_5$ for $NH_4VO_3$ as vanadium source can obtain more uniform ultrafine primary particles, compared with that of the previous work [14], and the spray-drying step bound these together via sucrose to form micron-sized spherical particles. The structure of the synthesized $Li_3V_2(PO_4)_3$/C favors the penetrating and soakage between the cathode material and electrolyte, decreases the diffusion length of lithium ions and electrons, and improves the processability of the $Li_3V_2(PO_4)_3$ cathode.

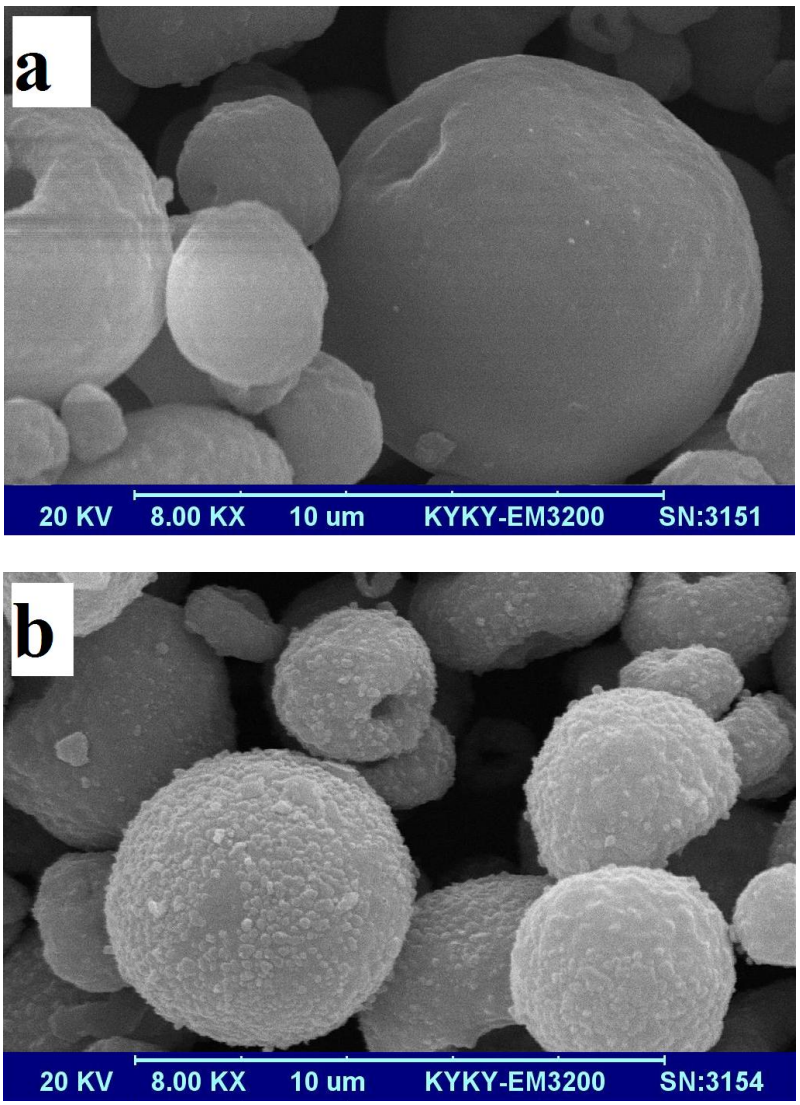


**Figure 3.** SEM images of the precursor powder (a) and $Li_3V_2(PO_4)_3$/C sample (b).

*3.2. Electrochemical results*

Shown in figure 4 is the charge–discharge behavior of the $Li_3V_2(PO_4)_3$ electrode operating at 0.2 C rate. As shown in figure 4a, the specific discharge capacity for the cathode active material is 131 mAh $g^{-1}$ and the charge–discharge profiles exhibit three charge plateaus and the corresponding three discharge ones, which corresponds to three compositional regions of $Li_{3-x}V_2(PO_4)_3$, that is, $x$ = 0.0–0.5, $x$ = 0.5–1.0 and $x$ = 1.0–2.0. The voltage plateau in each region corresponds to the reversed two-phase transition [6]. The differential capacity profile, shown in figure 4b, exhibits three peaks in deintercalation processes at 3.59, 3.67 and 4.09 V, and correspondingly three peaks in intercalation processes at 3.58, 3.66 and 4.04 V due to lithium insertion respectively. All the peaks are associated with $V^{3+}/V^{4+}$ redox couple, which is in good agreement with the charge-discharge behavior in figure 4a. Also the differential capacity profile indicates the excellent electrode reaction reversibility (as evidenced by the symmetrical nature of the deintercalation and intercalation responses) and the relatively low polarization (as shown by the small extent of voltage hysteresis).

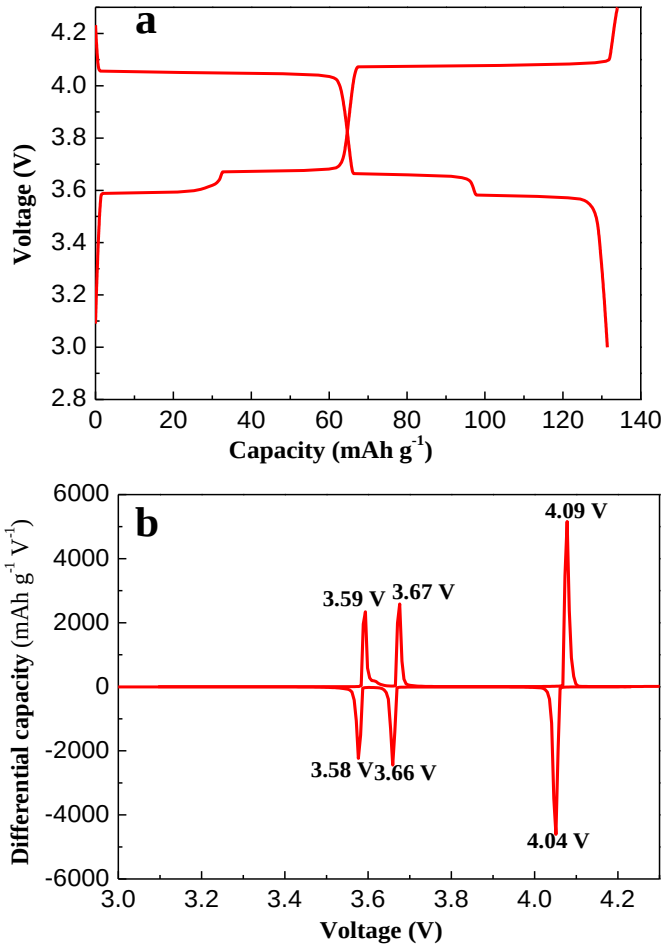


**Figure 4.** Charge/discharge profiles (a) and differential capacity curves (b) of the $Li_3V_2(PO_4)_3$/C electrode at 0.2 C rate in the voltage range of 3.0–4.3 V (1 C = 133 mA $g^{-1}$).

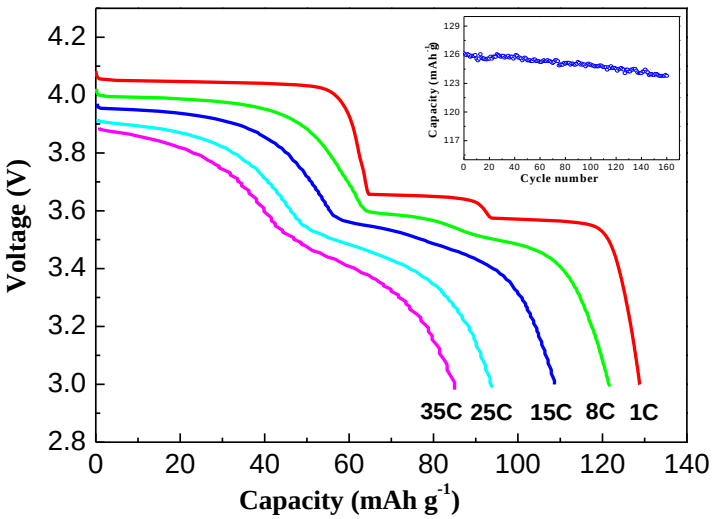


**Figure 5.** Initial discharge curves of $Li_3V_2(PO_4)_3$/C electrode at different rates. The insert shows the cycling stability curves of $Li_3V_2(PO_4)_3$/C materials.

Figure 5 demonstrates the rate performance of the as-prepared composite powders. The cells were charged to 4.3 V at 1 C rate, then discharged to 3.0 V at *n* C rate (where *n* = 1, 8, 15, 25, 35). As shown in figure 5, when the discharge current density increases from 1 to 35 C, the discharge capacity of 128, 121, 108, 93, 84 mAh $g^{-1}$ can still be achieved. Furthermore, there are significant voltage plateaus even when discharging at 35 C rate which is much better than that of the previous material [14]. This should be very attractive to development of high-power lithium-ion batteries. The cycling stability curve of the $Li_3V_2(PO_4)_3$/C material at 1 C charge and discharge rate, embedded in figure 5, indicates that following the 160 cycles the material retains 98% of the original specific capacity. The excellent cyclability and rate capability of the $Li_3V_2(PO_4)_3$/C composites can be attributed to the special hollow micro-spherical structure of the $Li_3V_2(PO_4)_3$/C composites. The spherical morphology with hollow structure improved the processability and wetting ability of the $Li_3V_2(PO_4)_3$ electrode. The nanosized particles shortened the diffusion length of lithium ions and electrons.

## 4. CONCLUSION

A novel hollow micro-spherical $Li_3V_2(PO_4)_3$/C composite has been successfully synthesized using a modified carbothermal reduction method. The $Li_3V_2(PO_4)_3$/C composite shows spherical morphology with hollow structure and contains a large number of nanosized primary particles. The rate performance and cyclability of the material are pretty good. The prepared composite is the promising material proposed as a cathode for high-power lithium-ion batteries.

ACKNOWLEDGMENTS
This work was supported by Doctoral Fund of Shandong Province (BS2009NJ001), the Project of Higher Educational Science and Technology Program of Shandong Province (J10LB56).

## References

1. M. Armand, J.M. Tarascon. *Nature.* 451 (2008) 652.
2. H.B. Thomas, A.F. *Andrew. Renew. Sust. Energ. Rev.* 13 (2009) 115.
3. B. Kang, G. Ceder. *Nature* 458 (2009) 190.
4. M.D. Cara, A.C. Rachel, M.S. Bernd, A. Philipp, J.D. Calum. *Chem. Mater.* 21 (2009) 5300.
5. J. Gao, J.J. Li, X.M. He, C.Y. Jiang, C.R. Wan. *Int. J. Electrochem.* 6 (2011) 2818.
6. M.Y. Saïdi, J. Barker, H. Huang, J.L. Swoyer, G. Adamson. *J. Power Sources* 119–121 (2003) 266.
7. H. Huang, S.C. Yin, T. Kerr, N. Taylor, L.F. Nazar. *Adv. Mater.* 14 (2002) 1525.
8. D. Morgan, G. Ceder, M.Y. Saïdi, J. Barker, J. Swoyer, H. Huang, G. Adamson. *Chem. Mater.* 14 (2002) 4684.
9. S.W. Oh, S.T. Myung, H.J. Bang, C.S. Yoon, K. Amine, Y.K. Sun. *Electrochem. Solid-State Lett.* 12 (2009) A181.
10. Y. Wang, G. Cao. *Adv. Mater.* 20 (2008) 2251.
11. M. Konarova, I. Taniguchi. *J. Power Sources* 194 (2009) 1029.
12. A. Pan, D. Choi, J. Zhan, S. Liang, G. Cao, Z. Nie, B.W. Arey, J. Liu. *J. Power Sources* 196

(2011) 3646.
13. B. Huang, X. Zheng, D. Jia, M. Lu. *Electrochim. Acta* 55 (2010) 1227.
14. B. Huang, X. Fan, X. Zheng, M. Lu. *J. Alloys Compd.* 509 (2011) 4765.
15. K.F. Hsu, S.Y. Tsay, B.J. Hwang. *J. Mater. Chem.* 14 (2004) 2690.
16. K. Edström, T. Gustafsson, J.O. Thomas. *Electrochim. Acta* 50 (2004) 397.
17. W. Li, B.L. Lucht. *J. Power Sources* 168 (2007) 258.
18. M. Ren, Z. Zhou, Y. Li, X. Gao, J. Yan. *J. Power Sources* 162 (2006) 1357.
19. M. Manickam, P. Singh, S. Thurgate, K. Prince. *J. Power Sources* 158 (2006) 646